the =C–F fluorines with chlorines, for example, the wavenumber drops[20] even when the C=C force constant is essentially unchanged.[27]

In both experimental studies[20,34] two a_1 bands near 1400 cm^{-1} were assigned based partly on the polarized nature of these bands in the Raman spectrum. Important indications of our theoretical calculations are (a) there should be only one a_1 fundamental at around 1400 cm^{-1} (ν_2), (b) the highest b_2 fundamental (ν_{18}) should also be placed in this region, (c) ν_3 (the third a_1 fundamental) is about 1150 cm^{-1} and has a very high depolarization ratio suggesting that it could be observed as depolarized in the Raman, and (d) still another b_2 fundamental should be found at a wavenumber as high as 1320 cm^{-1} (ν_{19}). It is disturbing that the experimental studies show all the bands around 1400 cm^{-1} (1420, 1383, and 1375 cm^{-1}; KNP) to be definitely polarized in the Raman; one possible candidate, however, as a combination band around 1380 cm^{-1} is ~980 cm^{-1} (b_2) + ~420 cm^{-1} (b_2).

The present theoretical results further suggest that the highest a_2 and b_1 fundamentals at HFCB are fairly near each other with wavenumbers about 1200 cm^{-1}. Thus, a band should be found in both the IR and Raman spectra of HFCB in this region. Furthermore, according to the calculated intensities, the highest b_1 fundamental (ν_{14}) should have the greatest intensity in the IR spectrum. The strongest and in the 1140–1340-cm^{-1} region is at 1174 cm^{-1} in the gas. Thus it seems reasonable to assign the band at 1174 cm^{-1} to ν_{14} and a somewhat higher wavenumber to ν_9.

The calculations are perfectly in line with all but three of KNP's assignments below 1000 cm^{-1}. The exceptions are ν_{10} (~120 cm^{-1}), ν_{15} (~70 cm^{-1}), and ν_{21} (~-70 cm^{-1}), where the differences in parentheses are theoretical minus experimental. It is very likely that the assignment of ν_{10} should be revised; however, experimental verification could be complicated by the fact that calculation predicts this band to almost coincide with ν_5. The experimental assignment of ν_{15} was quite uncertain[20] and the calculation predicts that it should be at a somewhat higher wavenumber. Lastly, from past experience it is quite unlikely that a force field calculation at the Hartree–Fock SCF level for a molecule like HFCB would place a fundamental at too low a wavenumber, which suggests a new assignment for ν_{21} may be in order.

Supplementary Material Available: From each plate: tables of total intensities, final backgrounds, and molecular intensities (15 pages). Ordering information is given on any current masthead page.

7-Azaindole and Its Clusters with Ar, CH₄, H₂O, NH₃, and Alcohols: Molecular Geometry, Cluster Geometry, and Nature of the First Excited Singlet Electronic State

Seong K. Kim and Elliot R. Bernstein*

Chemistry Department, Colorado State University, Fort Collins, Colorado 80523
(Received: September 11, 1989)

Mass-resolved excitation vibronic spectra of jet-cooled 7-azaindole and its clusters with Ar, CH₄, NH₃, H₂O, D₂O, CH₃OH, and C₂H₅OH are reported and analyzed with regard to molecular and cluster geometry and the nature of the first excited singlet state. Large changes in the various spectra are observed upon clustering and upon deuteration of 7-azaindole. The observed vibronic spectra of both 7-azaindole and its clusters can be rationalized with two general assumptions: (1) the hydrogen attached to the pyrrole nitrogen of 7-azaindole is out of the molecular plane in the first excited singlet state; and (2) the observed spectra are characterized by strong nπ*–ππ* mixing not completely removed by the clustering. MOPAC5 calculations of molecular geometry suggest that the S₁ state is nonplanar. Additional cluster potential energy calculations suggest that the formation of cyclic hydrogen-bonded clusters is not likely for these gas-phase 1:1 or 1:2 7-azaindole/solvent clusters: the major gas-phase solvent clustering probably takes place at the π-system of the 7-azaindole molecule.

I. Introduction

7-Azaindole (see Figure 1a, 7AZI) is suggested to have two very interesting and important properties in solution: (1) when solvated by hydrogen-bonding solvents (such as water, alcohols, ammonia, or even itself), it is thought to form a cyclic structure through a double hydrogen bond (Figure 1b);[1-3] and (2) it will tautomerize (Figure 1c) in protic solvent solutions via a cyclic hydrogen-bonded intermediate.[1,2,4-8] Such behavior is suggestive of the behavior of DNA bases,[9] and thus, 7AZI has been a particularly attractive and compelling system for study.

Spectra of isolated 7AZI and/or 7AZI clustered with various hydrogen-bonding and non-hydrogen-bonding solvents should aid in the elucidation of the energetics and dynamics involved in both the cyclic hydrogen-bonded solvation structures and in the tautomerization process. Supersonic jet expansion techniques coupled with laser spectroscopy and mass resolution (mass-resolved excitation spectroscopy) are, of course, an excellent experimental approach to the study of molecular and cluster structure and energetics. Through these techniques coupled with state of the art molecular orbital semiemperical calculations and potential energy cluster structure calculations, a good deal can be learned

(1) Taylor, C. A.; El-Bayoumi, M. A.; Kasha, M. *Proc. Natl. Acad. Sci. U.S.A.* **1969**, *63*, 253.
(2) Ingham, K. C.; El-Bayoumi, M. A. *J. Am. Chem. Soc.* **1974**, *96*, 1674.
(3) Stäglich, P.; Zander, M. *Z. Naturforsch.* **1976**, *31a*, 1391.
(4) Tokumura, K.; Watanabe, Y.; Itoh, M. *J. Phys. Chem.* **1986**, *90*, 2362. Tokumura, K.; Watanabe, Y.; Udagawa, M.; Itoh, M. *J. Am. Chem. Soc.* **1987**, *109*, 1346.
(5) bulska, H.; Chodkowsks, A. *J. Am. Chem. Soc.* **1980**, *80*, 3259.
(6) Hetherington, W. M.; Micheels, R. M.; Eisenthal, K. B. *Chem. Phys. Lett.* **1979**, *66*, 230.

(7) McMorrow, D.; Aartsma, T. J. *Chem. Phys. Lett.* **1986**, *125*, 581.
(8) Moog, R. S.; Bovino, S. C.; Simon, J. C. *J. Phys. Chem.* **1988**, *92*, 6545.
(9) Cantor, C. R.; Schimmel, P. R. *Biophysical Chemistry I*; Freeman: San Francisco, CA, 1980.
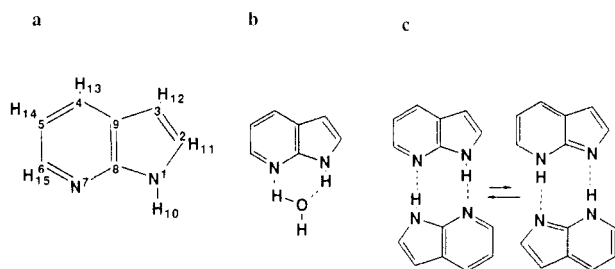
Figure 1. Structures of (a) 7AZI and (b) 7AZI/water cluster with a double-hydrogen-bonding structure, and (c) $(7AZI)_2$ and its possible tautomerization. The numbering on atoms in a is used in describing atoms in text and in Tables II, III, and IV.

about bare molecular and cluster static and dynamic properties.[10-13]

Spectra of jet-cooled 7AZI, $(7AZI)_2$, and 7AZI/water clusters have been previously obtained with a view toward the interpretation of the tautomerization process.[14-16] The cluster spectra evidence large red shifts from the bare molecule spectrum and are quite complex: in general, the bare molecule and the various cluster spectra do not appear to coincide with regard to either vibronic structure or intensity. These observations were attributed to double hydrogen bonding such as shown in Figure 1. Nevertheless, aside from this explanation, no firm evidence exists for such structure in the gas phase. In fact, evidence from other theoretical and experimental studies of isolated van der Waals (vdW) clusters[10-13] strongly suggests that the major interaction between aromatic (solute) molecules and small solvent (i.e., H_2O, NH_3, C_nH_{2n+2}, ROH, etc.) molecules is through the π-electron system of the solute and the major electron density of the solvent. For systems with a substantial hydrogen-bonding interaction in addition to the usual dispersion interaction, the cluster may have multiple stable structures: a planar hydrogen-bonding structure, a ring-centered π-electron/electron density structure, and a compromise structure in which neither form of interaction dominates the geometry.

In addition to the above likely complications of multiple cluster geometries for 7AZI clusters and dimers, the isolated molecule may evidence its own complicated spectral behavior due to three potential causes: (1) mixing between nearly degenerate ^1L_a and ^1L_b $\pi\pi^*$ excited electronic states; (2) mixing between the lowest $\pi\pi^*$ state (probably ^1L_b, which corresponds to the $^1B_{2u}$ state of benzene) and low-lying $n\pi^*$ states; and (3) nonplanarity of the 7AZI molecule in S_1, in particular, at the pyrrole nitrogen. The ^1L_b state with its dipole parallel to the long axis of the molecule is rather insensitive to the solvent environment while the ^1L_a state is lowered in energy by polar environments. In the case of 7AZI, both transitions are polarized more or less along the long molecular axis.[17] The ^1L_a and ^1L_b state are well separated in gas-phase indole[18] but are apparently close together in 7AZI.[1,19] For most isolated indole-like systems, only the ^1L_b state is identified at low energy. $n\pi^*-\pi\pi^*$ interactions have not been reported or documented for 7AZI but have been suggested for purines[20] and other systems.[21,22] A rotational analysis of the 0_0^0 transition for $S_1 \leftarrow S_0$[23] does not suggest any $n\pi^*-\pi\pi^*$ mixing, but almost all the
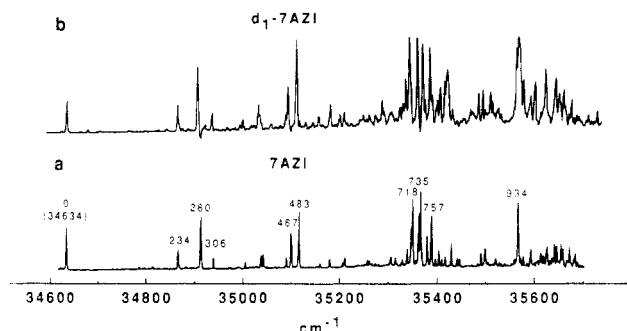

Figure 2. One-color TOFMS of (a) 7AZI and (b) 7AZI-d_1(H_{10}) for the region $0_0^0 + 1000$ cm^{-1}. The peak at 34 634 cm^{-1} is assigned as the 7AZI origin. The origin featuers are 2 or 3 times larger than shown.

transition intensity is expected to be of a $\pi\pi^*$ character.

The work reported in this paper addresses the above three complications for the S_1 state of bare and clustered 7AZI. Additionally, structures for 7AZI clusters with argon, methane, water, alcohols, and ammonia are suggested based on calculational and spectroscopic data.

II. Experimental Procedures

A detailed description of the supersonic jet/laser apparatus is found in ref 24. The doubled output of a pulsed Nd:YAG laser pumps a dye laser (R590, R610, KR620, R640, and SR640 plus DCM) whose output is in turn doubled into the ultraviolet in order to excite the samples of interest. The spectral range covered for a given sample often includes the output from several dyes so that relative intensities must be calibrated in overlapping dye regions. For such situations, the intensities are noted in the figure captions.

Mass-resolved excitation spectra (time-of-flight-mass spectroscopy, TOFMS) are obtained for all samples discussed in this report as the 7AZI (Aldrich, 98%) contains impurities that strongly absorb and emit light in the spectral regions of interest. These impurities could not be readily removed by recrystallization or vacuum sublimation. For the study of clusters, two-color TOFMS are needed to obtain clear spectra of clusters of specific stoichiometry.

7AZI is placed inside the head of a pulsed supersonic nozzle heated to ca. 70 °C. The expansion is generated with 50–70 psi of helium carrier gas. The solvents for clustering are either mixed with the carrier gas (gases) or placed in a trap before the nozzle.

7AZI-d_1 (at the pyrrole ring nitrogen—H_{10} on N_1, see Figure 1) is synthesized by mixing 7AZI (1%) with D_2O at room temperature, extracting the 7AZI-d_1 with ether, and drying the organic component in vacuum. NMR spectra taken of the sample confirm that only the most acidic hydrogen (H_{10} of Figure 1) is replaced.

III. Geometry Optimization Calculations

The geometry of the 7AZI molecule is calculated for the S_0 and S_1 electronic states with the molecular orbital package v. 5 (MOPAC5).[25] MOPAC5 uses the semiempirical MNDO method with optimized parametric Hamiltonians AM1[26] and PM3.[27] With a given set of input data for bond lengths and angles, the program optimizes molecular geometry and point-charge distributions over the atoms to obtain the minimum heat of formation. Additional molecular constants such as bond characteristics, dipole moment, and normal modes of vibration can also be found. These calculations are carried out for both the ground and first excited singlet states of 7AZI.

Two methods are employed to calculate the minimum energy geometries and binding energies for 7AZI/solvent clusters: the

(10) Nowak, R.; Menapace, J. A.; Bernstein, E. R. *J. Chem. Phys.* **1988**, *89*, 1309.

(11) Schauer, M.; Bernstein, E. R. *J. Chem. Phys.* **1985**, *82*, 726.

(12) Schauer, M.; Law, K. S.; Bernstein, E. R. *J. Chem. Phys.* **1985**, *82*, 736.

(13) Wanna, J.; Bernstein, E. R. *J. Chem. Phys.* **1986**, *84*, 927.

(14) Fuke, K.; Kaya, K. *J. Phys. Chem.* **1989**, *93*, 614.

(15) Fuke, K.; Yoshiuchi, H.; Kaya, K. *J. Phys. Chem.* **1984**, *88*, 5840.

(16) Ruane, T. P. Thesis, Princeton University, 1987.

(17) Catalan, J.; Perez, P. *J. Theor. Biol.* **1979**, *81*, 213.

(18) Bersohn, R.; Even, U.; Jortner, J. *J. Chem. Phys.* **1984**, *80*, 1050.

(19) Wagner, R. W. Thesis, Michigan State University, 1971.

(20) Clark, L. B.; Tinoco, L. *J. Am. Chem. Soc.* **1965**, *87*, 11.

(21) Wanna, J.; Bernstein, E. R. *J. Chem. Phys.* **1987**, *86*, 6707.

(22) Nimlos, M. R.; Kelley, D. F.; Bernstein, E. R. *J. Phys. Chem.* **1989**, *93*, 643.

(23) Bryant, P.; Hollas, J. M. *Indian J. Phys.* **1986**, *60B*, 1.

(24) Bernstein, E. R.; Law, K.; Schauer, M. *J. Chem. Phys.* **1984**, *80*, 207.

(25) Stewart, J. J. P. MOPAC, A General Molecular Orbital Package, 5th ed., 1988.

(26) Dewar, M. J. S.; Zoebisch, E. G.; Healy, E. F.; Stewart, J. J. P. *J. Am. Chem. Soc.* **1985**, *107*, 3902.

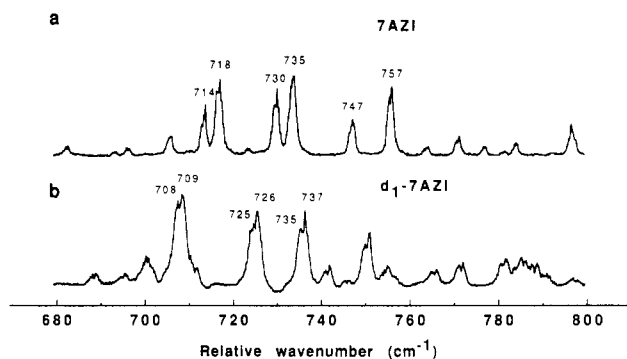(27) Stewart, J. J. P. *J. Comput. Chem.* **1989**, *10*, 209, 221.

Figure 3. One-color TOFMS of (a) 7AZI and (b) 7AZI-d_1 with an expanded energy scale. Note the collapse of 7AZI doublet structure in this region upon H$_{10}$ dueteration.

above MOPAC5 program and a potential energy calculation based on Lennard-Jones, hydrogen bonding, and coulomb atom–atom interactions.[28] These latter calculations are well described in our previous publications.[22]

Input data for the potential energy cluster calculations are the potential parameters for the different forms of interactions and different atoms and the bond angles, bond lengths and atomic charges for all the molecules. These molecular data come from MOPAC5 AM1 and PM3 Hamiltonian calculations.

IV. Results and Discussion

A. 7-Azaindole—Spectroscopy. The one-color TOFMS of 7AZI is presented in Figure 2. The intense feature at 34634 cm^{-1} is believed to be the S$_1$ ← S$_0$ transition origin. Low-energy vibronic features, which play a major role in our overall analysis of the bare molecule and cluster spectra, are assigned at 234, 280, 306, 467, and 483 cm^{-1}. Prominent doublets are identified in this spectrum at 714, 718 and 730, 735 cm^{-1}, and an intense feature is located at 934 cm^{-1}. Upon deuteration of 7AZI at the acidic H$_{10}$ position (7AZI-d_1), two changes are found in the 7AZI spectrum: (1) many of the low-frequency modes shift to lower energy by as much as 3% (Figure 2b); and (2) the doublets in the spectrum collapse (Figure 3). These changes are tabulated in Table I. Both of the above observations are quite unusual in a qualitative and quantitative sense for a "normal" aromatic S$_1$ ← S$_0$ transition.[29] Additionally, the 7AZI spectrum displays a large number of vibronic features of quite weak intensity, which are not very obvious from the figures. This is another striking aspect of the 7AZI spectrum.

Upon comparing the 7AZI spectrum with that of indole,[18,30] one finds few common features. The vibronic features between 700 and 800 cm^{-1} are similar for both molecules, but the doublet structure here and throughout the spectrum (for weaker features) is unique to 7AZI. The low-energy peaks at 234, 280, 306, 467, and 483 cm^{-1} are also unique to 7AZI. These differences between the two spectra are surprising considering the S$_1$ ← S$_0$ transition is supposed to be to the same ππ* ^{1}L$_b$ S$_1$ state in both instances. Moreover, indole has only 2 weak vibronic features below 600 cm^{-1},[18,30] while 7AZI has more than 13 relatively intense low-energy features.

The unusually large number of low-lying vibronic features for 7AZI and the difference between the 7AZI, 7AZI-d_1, and indole spectra can be accounted for by two molecular properties of 7AZI: (1) the molecule is nonplanar in S$_1$, particularly at the N$_1$–H$_{10}$ pyrrolic site; and (2) strong nπ*–ππ* vibronic mixing occurs in the region of the S$_1$ ← S$_0$ transition.

The nonplanarity of 7AZI in the S$_1$ state (in particular at H$_{10}$) would account for the large deuterium substitution (shifts and collapse of doublets) effect on the spectrum and might also lead

(28) Nemethy, G.; Pottle, M. S.; Scherga, H. A. *J. Phys. Chem.* **1983**, *87*, 188. Momany, F. A.; Carruthers, L. M.; McGuire, R. F.; Scherga, H. A. *J. Phys. Chem.* **1974**, *78*, 1595.

(29) *Atomic and Molecular Clusters*; Bernstein, E. R., Ed.; Elsevier: Amsterdam, 1990.

(30) Hager, J.; Wallace, S. C. *J. Phys. Chem.* **1983**, *87*, 2121.

TABLE I: Deuterium Substitution (H$_{10}$, See Figure 1) Effect on Vibrational Energies of 7AZI^a

vibrational energies/cm^{-1}		
7AZI	7AZI-d_1	intensity
0 (34634)	0 (34637)	vs, 0^0_0 origin
234	230	m
280	272	s
306	301	m
372	366	w
404, 409	397, 400	w
457	453	w
467	458	m
483	475	s
527	523	w
547	545	w
574, 578	567, 573	w
672	652	w
682	688	w
696	695	w
706	700	w
714, 718	708, 709	m
730, 735	725, 726	s
747	735, 736	m
757	742, 743	s
772	750, 752	w
796		m
857, 866	851, 859	w
934	934	s

^{a} Not all weak peaks after 700 cm^{-1} are tabulated.

to an increased number of allowed vibronic transitions. Even this nonplanarity, however, should not give rise directly to so many transitions.

We suggest that a strong nπ*–ππ* mixing would account for the apparent density of vibronic transitions in the S$_1$ ← S$_0$ manifold. Similar suggestions have been made for isoquinoline,[21,31] quinoline,[21] 2-hydroxypyridine,[22] and other molecules. The intensity of these vibronic transitions comes from the ππ* state but the peak positions are associated with nπ*–ππ* vibronic resonances and couplings. As in the case of isoquinoline, we are unable to detect direct absorption (through either TOFMS or FE experiments) from S$_0$ to the nπ* excited state.

In order to elucidate this problem further, two approaches are useful: (1) calculation of the S$_0$ and S$_1$ geometry and (2) clustering of 7AZI with various solvents to alter the nπ*–ππ* coupling and perhaps to affect the 7AZI planarity.

B. 7-Azaindole—Calculations. The geometry and atomic point-charge distribution for 7AZI in both the ground and first excited singlet states are calculated with MOPAC5 AM1 and PM3 Hamiltonians. These data are summarized in Tables II and III. The optimum geometries calculated with either Hamiltonian are the same for the ground state, although significant differences are found for the atomic partial charges at various atoms (e.g., C$_9$ and N$_1$). For the first excited state, the two Hamiltonians give different geometries: the AM1 Hamiltonian yields a nonplanar molecule (C$_9$ and H$_{10}$) while the PM3 Hamiltonian yields a planar molecule. These calculations, however, are neither very accurate nor reliable as the convergence criteria for optimum S$_1$ geometry for both these calculations is poor ($\approx$7 for S$_1$ as opposed to 0.01 for S$_0$). Moreover, different optimum geometries obtain for different initial input geometries. The general trend of results for the AM1 calculations seems sound, however; 7AZI apparently has a propensity for nonplanarity of the pyrrolic ring in S$_1$, especially at C$_9$ and H$_{10}$. The AM1 Hamiltonian can generate a nonplanar 7AZI for the first excited singlet state. H$_{10}$ is typically out of plane by 18–19° (see Figure 4).

We can conclude from both the experimental and theoretical results that some of the spectral crowding and doubling of various vibronic features in the 7AZI spectrum may well be due to the loss of planarity in S$_1$. The potential well for H$_{10}$ motion with

(31) Hiraya, A.; Achiba, Y.; Kimura, K.; Lim, E. C. *J. Chem. Phys.* **1984**, *81*, 3345.

TABLE II: Optimum Geometry and Charge Distribution for 7AZI in the Ground State, Results from MOPAC5 Calculations Using the PM3 and AM1 Hamiltonians

atom I^a	bond length/Å		bond angle/deg		twist angle/deg		J	K	L^b	charge (e)	
	PM3	AM1	PM3	AM1	PM3	AM1				PM3	AM1
1N										0.3155	−0.2033
2C	1.410	1.397					1			−0.2419	−0.0762
3C	1.381	1.392	109.27	110.59			2	1		−0.1466	−0.1921
4C	1.403	1.396	134.72	135.68	−179.93	180.00	9	3	2	−0.0035	−0.0420
5C	1.378	1.386	117.62	117.99	179.98	180.00	4	9	3	−0.1871	−0.2116
6C	1.417	1.419	120.96	119.86	0.01	0.03	5	4	9	−0.0454	−0.0530
7N	1.337	1.336	123.17	125.34	−0.02	−0.02	6	5	4	−0.0687	−0.1454
8C	1.402	1.402	107.95	108.14	0.15	0.09	1	2	3	−0.1681	0.0281
9C	1.424	1.459	107.87	107.59	0.12	−0.07	8	1	2	−0.1300	−0.1210
10H	0.987	0.985	125.66	126.46	179.55	179.87	1	2	3	0.0768	0.2592
11H	1.090	1.092	128.40	129.33	179.98	179.98	2	3	9	0.1400	0.1676
12H	1.087	1.085	126.77	126.79	179.91	179.96	3	2	1	0.1285	0.1587
13H	1.094	1.099	120.50	120.58	180.01	179.99	4	9	8	0.1061	0.1386
14H	1.094	1.097	120.43	120.95	180.00	180.02	5	4	9	0.1118	0.1407
15H	1.096	1.106	121.34	119.75	179.99	179.99	6	5	4	0.1125	0.1568

final heat of formation: 48.15 kcal/mol for PM3; 66.97 kcal/mol for AM1
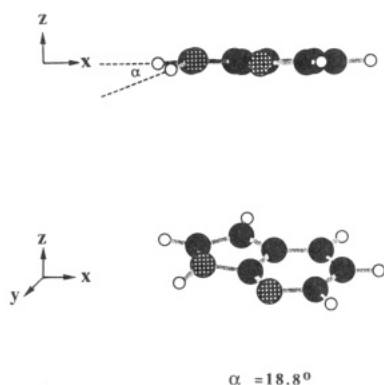
^{a} Numbering of atoms are as specified in Figure 1a. ^{b} The bond length is defined between I and J. The bond angle is defined between lines IJ and JK. The twisting angle is defined between plane JKL and line IJ.

TABLE III: Optimum Geometry and Charge Distribution for 7AZI in the First Excited Singlet State, Results from MOPAC5 Calculations Using the PM3 and AM1 Hamiltonians^a

atom I	bond length/Å		bond angle/deg		twist angle/deg		J	K	L	charge (e)	
	PM3	AM1	PM3	AM1	PM3	AM1				PM3	AM1
1N										0.4769	−0.1686
2C	1.364	1.362					1			−0.4079	−0.1737
3C	1.436	1.459	108.34	110.04			2	1		−0.0031	−0.0743
4C	1.385	1.404	134.98	134.96	−179.80	179.85	9	3	2	−0.1176	−0.1329
5C	1.418	1.404	117.18	116.89	179.82	−179.88	4	9	3	−0.1255	−0.1619
6C	1.377	1.395	121.63	120.82	0.08	1.22	5	4	9	−0.0854	−0.0926
7N	1.395	1.365	122.88	125.20	0.01	−0.42	6	5	4	−0.1268	−0.1743
8C	1.422	1.446	109.76	108.23	−0.18	−3.57	1	2	3	−0.1590	0.0887
9C	1.422	1.454	107.31	107.23	0.20	4.20	8	1	2	−0.1307	−0.1330
10H	0.986	0.993	125.28	126.47	179.86	−161.22	1	2	3	0.0648	0.2510
11H	1.092	1.092	126.66	127.26	179.95	−176.44	2	3	9	0.1585	0.1760
12H	1.088	1.085	125.65	125.26	179.95	−177.45	3	2	1	0.1252	0.1630
13H	1.092	1.095	121.73	121.37	179.93	177.86	4	9	8	0.1111	0.1393
14H	1.094	1.099	118.59	119.66	180.03	−178.98	5	4	9	0.1047	0.1267
15H	1.094	1.105	123.41	121.08	180.02	−178.85	6	5	4	0.1147	0.1562

final heat of formation: 145.81 kcal/mol for PM3; 170.05 kcal/mol for AM1
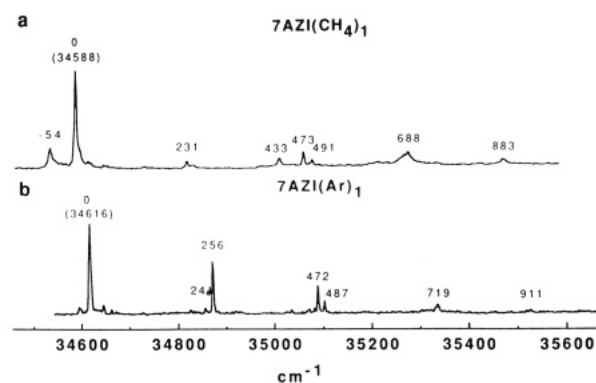
^{a} See footnotes given in Table II.

$\alpha = 18.8°$

Figure 4. MOPAC5 result for the first excited singlet state geometry of 7AZI, employing the AM1 Hamiltonian.

Figure 5. Two-color TOFMS of (a) 7AZI(CH₄)₁ and (b) 7AZI(Ar)₁. Wavelength for the ionizing laser is 3200 Å.

respect to the plane of the heavy atom ring is probably a double well with a barrier to the zero-degree, planar conformation.

C. 7-Azaindole $(Ar)_1$ and $(CH_4)_1$ Clusters. The general reason to look at cluster spectra at this point is to resolve the two issues posed above: (1) the (S_1) nonplanarity of 7AZI and its ensuing double-well potential surface and (2) the importance of $n\pi^*-\pi\pi^*$ mixing for this molecule.

Spectra for 7AZI(Ar)₁ and (CH₄)₁ are presented in Figure 5. The cluster shifts for the 0_0^0 transition are −18 cm^{-1} for 7AZI(Ar)₁ and −46 cm^{-1} for 7AZI(CH₄)₁. These are quite typical of cluster

shifts for other solute systems. For example for toluene, pyrazine, pyrimidine, benzene, and indole the origin shift for 1:1 methane clusters are −43,[12] −33,[13] −57,[32] −41,[11] and −36[33] cm^{-1}, respectively, and the shifts for benzene and indole with argon are −21[34] and −26[35] cm^{-1}, respectively.

(32) Wanna, J.; Menapace, J. A.; Bernstein, E. R. *J. Chem. Phys.* **1986**, *85*, 1795.

(33) Hager, J.; Ivanco, M.; Smith, M. A.; Wallace, S. C. *Chem. Phys. Lett.* **1985**, *113*, 503.

(34) Stephenson, T. A.; Rice, S. A. *J. Chem. Phys.* **1984**, *81*, 1083.
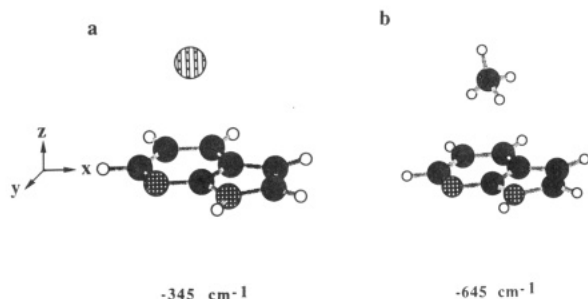
Figure 6. Optimum geometries for $7AZI(Ar)_1$ and $7AZI(CH_4)_1$ obtained with a potential energy calculation. Both PM3 and AM1 7AZI structures and charges result in identical cluster geometries. Also shown are cluster binding energies.
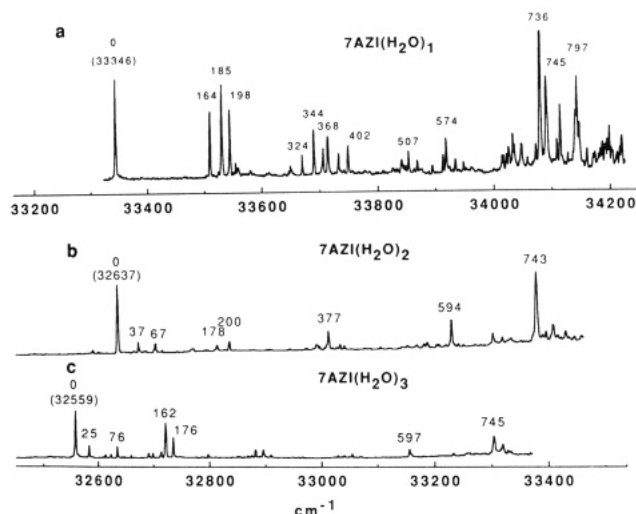

Figure 7. One-color TOFMS of (a) $7AZI(H_2O)_1$ and (b) $7AZI(H_2O)_2$. The peaks between 33 200 and 33 400 cm⁻¹ are 2–3 times larger than shown.

$\alpha = 136.1°$ $\beta = 83.8°$ $\gamma = 135.8°$

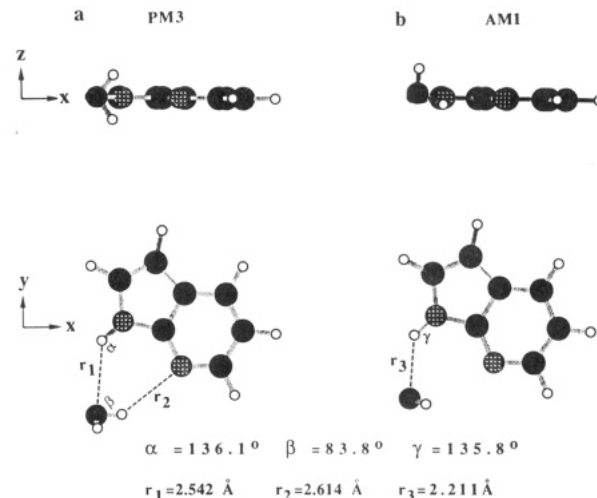$r_1 = 2.542$ Å $r_2 = 2.614$ Å $r_3 = 2.211$ Å

Figure 8. MOPAC5 results for the local hydrogen-bonding structure of $7AZI(H_2O)_1$, using (a) PM3 and (b) AM1 Hamiltonians.

red-shifted by 1997 and 2075 cm⁻¹, respectively. These red shifts are enormous considering those found for benzene[32] (+85 cm⁻¹), indole[37] (−135 cm⁻¹), phenol[38] (−356 cm⁻¹), fluorene[39] (+57 cm⁻¹), and isoquinoline[21] (0.6 cm⁻¹) clusters with $(H_2O)_1$. The unusually large red shift for 7AZI/water clusters suggests that the $n\pi^*$–$\pi\pi^*$ excited-state interaction has been (at least partially) removed by the interaction of 7AZI with water. Hydrogen-bonding solvents are known to raise the energy of $n\pi^*$ states with respect to $\pi\pi^*$ states.[40] The suggested mechanism for this increase in the $n\pi^*$ excitation energy is the lowering of the ground-state n orbital energy due to hydrogen bond formation between water and the lone pair electrons on the ring nitrogen (see Figure 1b). If the $n\pi^*$ state were raised in energy above the $\pi\pi^*$ state, additional lowering in energy of the $\pi\pi^*$ state would occur through interaction between these two zero-order descriptions.

Not only is the origin shift of 7AZI/water clusters with respect to 7AZI suggestive of excited electronic state mixing but the observed cluster vibronic structure is as well. Note that the low-energy modes of 7AZI S_1 have changed nearly 33% in $7AZI(H_2O)_1$: this is almost unique for vdW clusters. Apparent overtone structure is observed for both systems. The strong 7AZI feature at 934 cm⁻¹ is missing in $7AZI(H_2O)_n$ spectra; vibrational predissociation is unlikely to be the reason for this absent feature based on binding energy considerations.

Given the large cluster shifts, the change in S_1 vibrational structure upon clustering with water, and the absence of any other 7AZI/water features in the 33 000–36 000-cm⁻¹ region, we believe that the excited state observed for 7AZI/water is ^1L_b with a significant removal of $n\pi^*$-state interference. The ^1L_a state is probably not observed in this region.

Cluster structure has been explored through a number of different calculations. Both MOPAC5 and potential energy calculations are performed on the $7AZI(H_2O)_1$ clusters. Table IV and Figures 8 and 9 summarize the results of such studies. The MOPAC5 calculation gives distorted double-hydrogen-bonded structures for the PM3 Hamiltonian (Figure 8a) but single-hydrogen-bonded structures for the AM1 Hamiltonian (Figure 8b). In neither case is the water nor the 7AZI structures and charges much different from those of the isolated individual molecules. Note that the MOPAC5 calculation [tested in this study for the pyrazine[41] and pyrimidine[41] dimers and pyrazine(NH₃)₁[32]] tends to underestimate the vdW dispersion interaction between the

Calculations of cluster geometry are presented in Figure 6. Again, very typical behavior is observed for the single minimum energy configurations of these clusters.

By contrast, comparison of the vibrational structure of these clusters with each other and bare 7AZI shows substantial changes in the vibronic features brought about by clustering. This is strong evidence that $n\pi^*$–$\pi\pi^*$ mixing is distorting the observed cluster and bare molecule vibronic structure. Thus, the apparent density of vibronic features in the 7AZI bare molecule spectrum may well be due to vibronic coupling between a low-lying $n\pi^*$ state and the "observed" $\pi\pi^*$ state "S_1". The observed vibronic transitions in this region can reflect this interaction and not existing vibrational structure in the 7AZI excited $\pi\pi^*$ electronic state.

At higher vibrational levels in S_1, the transition intensity of both clusters begins to decrease due to vibrational predissociation of the clusters.[36] The intense feature at +934 cm⁻¹ above the 0_0^0 transition of the bare molecule is no longer observed due to either vibrational predissociation or removal of the $n\pi^*$–$\pi\pi^*$ interaction upon clustering. In either event, this demonstrates that the 934-cm⁻¹ feature is a vibronic one and not a new electronic origin (e.g., ^1L_a). Thus, the observed spectra are suggested to be due to a transition involving the ^1L_b ($\pi\pi^*$). The excited ^1L_b ($\pi\pi^*$) state probably interacts with a lower energy singlet $n\pi^*$ state to produce the observed complex high-density $S_1 \leftarrow S_0$ transition in the 34 600–35 600-cm⁻¹ region.

D. 7-Azaindole/H₂O Clusters. The spectra of $7AZI(H_2O)_{1,2,3}$ are presented in Figure 7. The 0_0^0 transition for $7AZI(H_2O)_1$ is located at 33 346 cm⁻¹, red-shifted by 1288 cm⁻¹ from the bare molecule 0_0^0 transition. The $7AZI(H_2O)_{2,3}$ spectra are further

(35) Hager, J.; Wallace, S. C. *J. Phys. Chem.* **1984**, *88*, 5513.
(36) Kelley, D. F.; Bernstein, E. R. *J. Phys. Chem.* **1986**, *90*, 5164.

(37) Montoro, T.; Jourvet, C.; Campillo, A. L.; Soep, B. *J. Phys. Chem.* **1983**, *87*, 3582.
(38) Fuke, K.; Kaya, K. *Chem. Phys. Lett.* **1983**, *94*, 97.
(39) Im, H. S.; Grassian, V. H.; Bernstein, E. R. *J. Phys. Chem.* **1990**, *94*, 222.
(40) See ref 21 and references quoted therein.
(41) Wanna, J.; Menapace, J. A.; Bernstein, E. R. *J. Chem. Phys.* **1986**, *85*, 777.
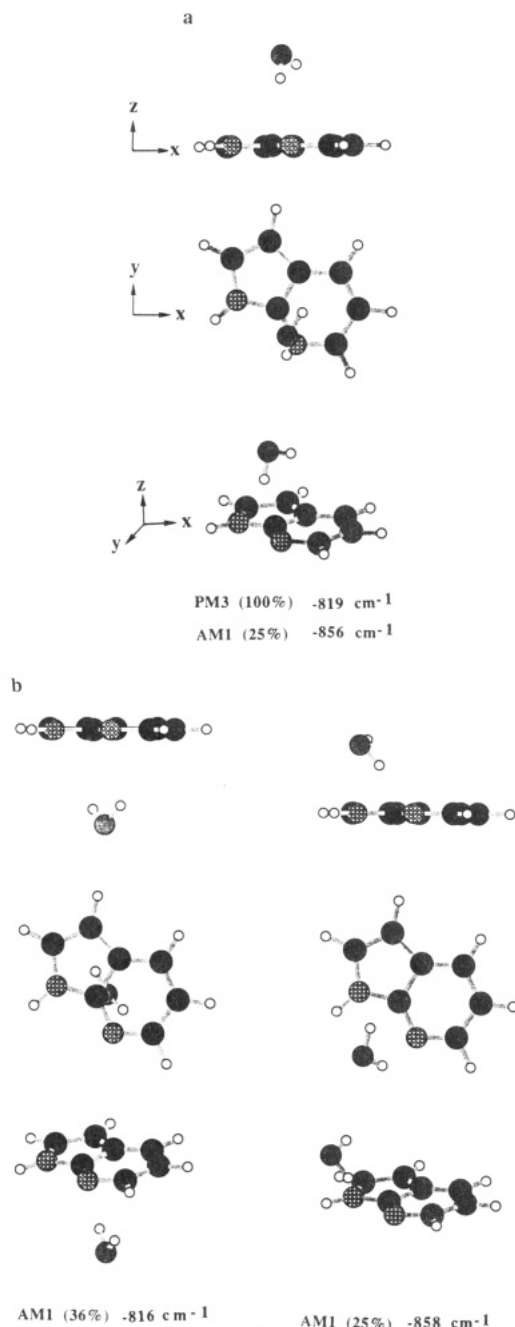
a

PM3 (100%)　-819 cm^{-1}

AM1 (25%)　-856 cm^{-1}

b

AM1 (36%)　-816 cm^{-1}　　　AM1 (25%)　-858 cm^{-1}

Figure 9. Potential energy calculation results for 7AZI(H$_2$O), using (a) PM3 molecular structures and charges and (b) AM1 structures and charges. The percentages listed in the figure refer to the number of times each structure is found, starting from random initial molecular positions and orientations. Also shown are the cluster binding energies and the percentages of the outcomes.

aromatic π-system and the solvent heavy atom(s). In general, these structures do not appear to be very reliable.

The potential energy calculation (Figure 9) generates different structures for 7AZI(H$_2$O)$_1$, depending on the Hamiltonian employed for the isolated molecule structure calculations. The PM3 molecules generate a single structure while the AM1 molecules yield three different structures, one of which is the PM3 structure. Nevertheless, all of these structures are the basic compromise structure falling between those found for only hydrogen bonding interactions and those found for only dispersion interactions. If a double-hydrogen-bonded structure (Figure 8a) is fixed for the potential energy calculation as an initial geometry, a binding energy of ca. 560 cm^{-1} is obtained; this structure is, however, not a minimum on the potential surface. Such minimum energy structures are presented in Figure 9. This of course makes a good deal of "intuitive sense". We believe that these geometries are
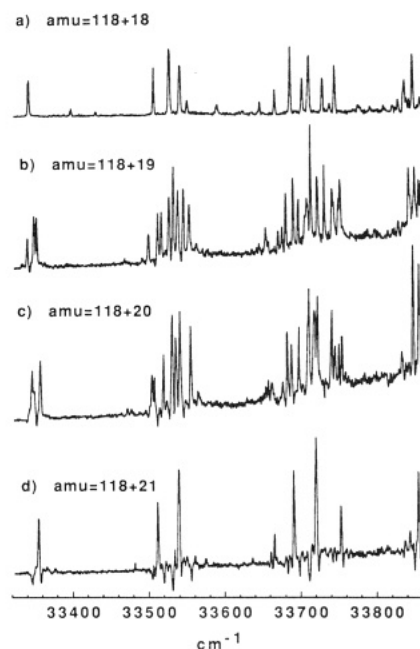

Figure 10. One-color TOFMS of 7AZI clustered with D$_2$O. Detection mass channels are indicated in each spectrum.

more reliable than either the PM3 or AM1 MOPAC5 cluster/dimer geometries (Figure 8).

Potential energy calculations for higher order clusters, based on PM3 molecules, generate two significant results: a plethora of structures and, if the ring center positions are occupied, a double-hydrogen-bonded cyclic structure. The suggestion here is that the largest interaction between 7AZI and water is at the π-system of 7AZI but that once these positions are occupied the hydrogen bonding structures (cyclic and otherwise) can be realized.

E. 7-Azaindole/D$_2$O Clusters. If D$_2$O is substituted for H$_2$O in the expansion system mixture, mass-resolved excitation spectra are observed for 7AZI (118), (118 + 1), (118 + 18), (118 + 19), (118 + 20), and (118 + 21) amu, etc. The spectra at mass channels (118 + 1) and (118 + 18) amu are identical with those of 7AZI-d_1 and 7AZI(H$_2$O)$_1$, respectively. Spectra taken at mass channels (118 + 18), (118 + 19), (118 + 20), and (118 + 21) amu are presented in Figure 10. The spectra certainly suggest that a rapid exchange between the acidic H$_{10}$ of 7AZI and the protons of water takes place on the S$_0$ potential surface. Thus, the spectrum of Figure 10b is composed of 7AZI-d_1(H$_2$O)$_1$ and 7AZI(HOD)$_1$ spectra, and the spectrum of Figure 10c is composed of 7AZI-d_1(HOD)$_1$ and 7AZI(D$_2$O)$_1$ spectra. The spectrum taken at mass channel (118 + 21) amu (Figure 10d) is then due to 7AZI-d_1(D$_2$O)$_1$. The ratio of peak heights in these spectra is roughly that expected for the statistical distribution of the various isotopic cluster species.

Two features of Figure 10 are worth special emphasis. First, both spectra at (118 + 19) and (118 + 20) amu consist of three-origin transition: three origins, of course, implies the existence of three distinct sites for the deuterium substitution. The three sites are most likely H$_{10}$ of 7AZI (as found specifically for this particular deuteration) and the two distinct proton sites on the water molecule in the cluster. This experimental observation is not consistent with the AM1 MOPAC5 geometry depicted in Figure 8b. Second, the spectrum of 7AZI-d_1(D$_2$O)$_1$ is much simpler (fewer transitions) than that of 7AZI(H$_2$O)$_1$ (compare Figure 10a,d). The nπ*–ππ* interaction suggested above for 7AZI may thus not be totally removed even in the presence of water solvation. This is perhaps further evidence against a strong hydrogen-bonded cyclic structure for 7AZI(H$_2$O)$_1$ as generated by the PM3 MOPAC5 cluster calculation (Figure 8a).

Figure 11 shows the spectrum taken at mass channel (118 + 37). This mass corresponds to 7AZI plus two waters with one of the water hydrogens or H$_{10}$ a deuterium. The five possible conformers due to the different deuterium substitution sites appear

TABLE IV: Optimum Geometry and Charge Distribution for 7AZI(H₂O)₁ in the Ground State, Results from MOPAC5 Calculations Using the PM3 and AM1 Hamiltonians[a]

atom I	bond length/Å		bond angle/deg		twist angle/deg		J	K	L	charge (e)	
	PM3	AM1	PM3	AM1	PM3	AM1				PM3	AM1
1N										0.3152	−0.2024
2C	1.409	1.394					1			−0.2368	−0.0710
3C	1.381	1.392	109.35	110.57			2	1		−0.1505	−0.1988
4C	1.398	1.396	134.82	135.89	−179.70	179.94	9	3	2	0.0014	−0.0441
5C	1.379	1.387	117.63	118.01	−179.86	−179.89	4	9	3	0.1900	−0.2133
6C	1.416	1.418	120.96	119.89	0.09	0.03	5	4	9	−0.0428	−0.0517
7N	1.338	1.336	123.22	125.30	−0.05	0.00	6	5	4	−0.0882	−0.1728
8C	1.402	1.402	107.88	108.04	0.63	0.01	1	2	3	−0.1692	0.0232
9C	1.427	1.460	108.05	107.71	−0.30	0.02	8	1	2	−0.1299	−0.1189
10H	0.989	0.993	125.90	126.89	179.34	−179.90	1	2	3	0.0930	0.2809
11H	1.090	1.092	128.40	129.26	179.98	180.00	2	3	9	0.1410	0.1692
12H	1.087	1.085	126.80	126.81	179.80	180.03	3	2	1	0.1288	0.1586
13H	1.094	1.099	120.52	120.59	179.97	180.01	4	9	8	0.1064	0.1391
14H	1.094	1.097	120.45	120.95	180.02	179.98	5	4	9	0.1124	0.1409
15H	1.096	1.106	121.28	119.68	179.89	180.00	6	5	4	0.1105	0.1540
16O	3.352	3.083	150.22	156.81	−174.78	179.76	7	6	5	−0.3851	−0.4082
17H	0.953	0.962	33.93	66.66	−44.12	−61.76	16	7	6	0.2002	0.2075
18H	0.951	0.962	107.61	103.36	−86.61	−49.24	16	17	7	0.1835	0.2075

final heat of formation: −7.71 kcal/mol for PM3; 1.04 kcal/mol for AM1

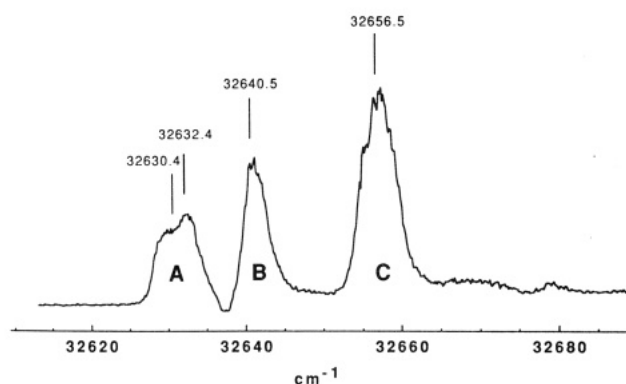[a] See footnotes given in Table II.

Figure 11. One-color TOFMS of 7AZI clustered with D₂O, detected at mass channel (118 + 37). (See text for a discussion of the doublet (A, C) and singlet features.)
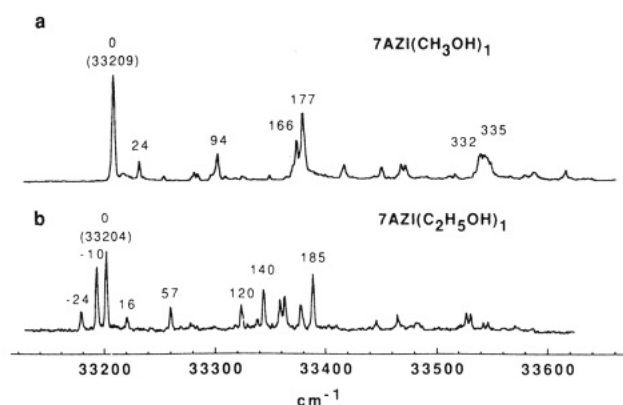

Figure 12. Two-color TOFMS of (a) 7AZI(CH₃OH)₁ and (b) 7AZI-(C₂H₅OH)₁. Wavelength of the ionizing laser is 3225 Å.

in three distinctive bands of electronic origins. The band B apparently represents a single peak and can be tentatively assigned to 7AZI-d_1(H₂O)₂, while each of bands A and C is apparently composed of two very close peaks and can tentatively be assigned to 7AZI(H₂O)(DOH). Attempts to identify the structure of 7AZI plus two waters from Figure 11 meet with some difficulty; however, we believe that if the double-hydrogen-bonding structure in Figure 8a were realistic, four distinctive bands would be observed at mass channel (118 + 37) for the cluster origin.

F. 7-Azaindole/Alcohol Clusters. Figure 12 shows the two-color TOFMS of 7AZI(CH₃OH)₁ and 7AZI(C₂H₅OH)₁.
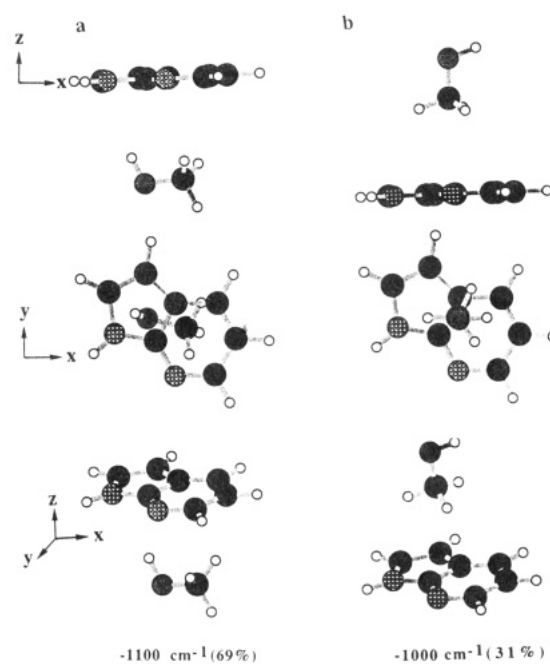

Figure 13. Potential energy calculation result for the geometry of 7AZI(CH₃OH)₁. PM3 molecules are used.
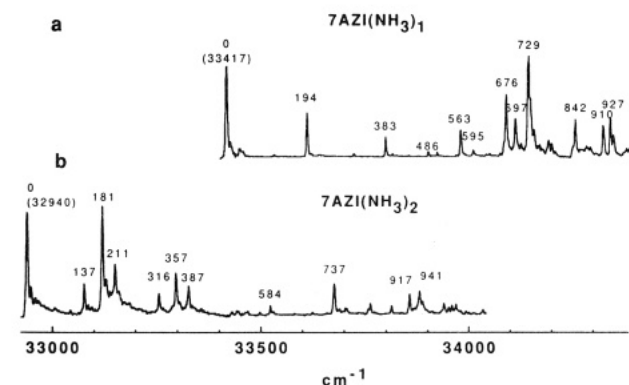

Figure 14. Two-color TOFMS of (a) 7AZI(NH₃)₁ and (b) 7AZI-(NH₃)₂. Wavelength of the ionizing laser is 3244 Å.

7AZI(CH₃OH)₁ displays a single origin while 7AZI(C₂H₅OH)₁ shows multiple origins. The spectra do not display common
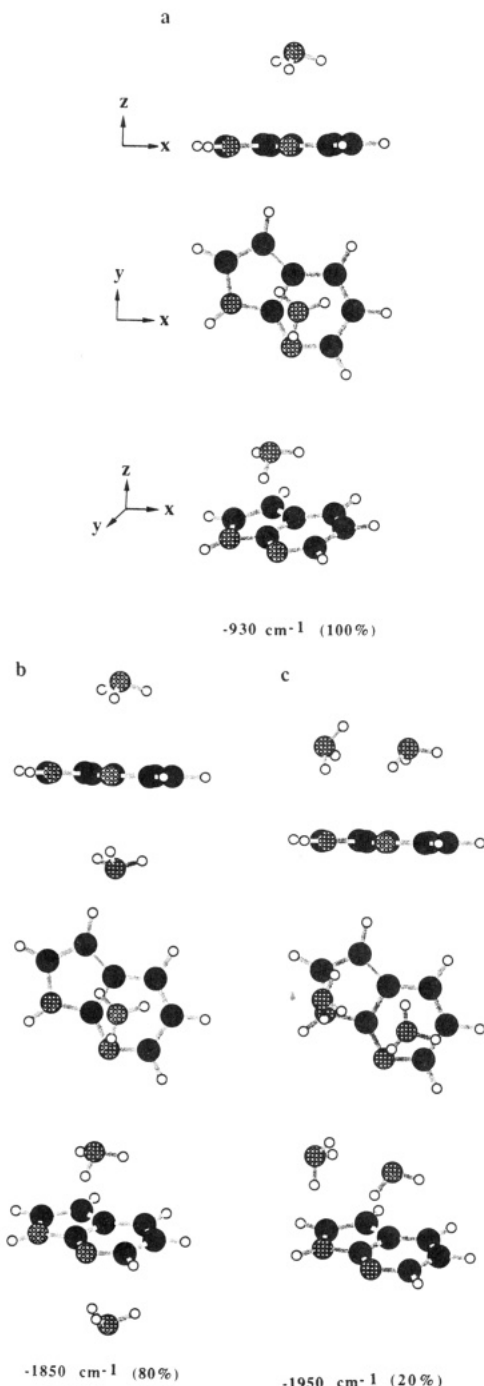
a

-930 cm⁻¹ (100%)

b   c

-1850 cm⁻¹ (80%)   -1950 cm⁻¹ (20%)

Figure 15. Potential energy calculation results (based on PM3 molecules) for (a) 7AZI(NH₃)₁ and (b) 7AZI(NH₃)₂.

vibronic features, again suggesting that the $n\pi^*-\pi\pi^*$ interaction has not been removed in these clusters.

The potential energy calculations for 7AZI(CH₃OH)₁ are presented in Figure 13. Two structures are found for this system. The hydrogen bonding interaction weakens for ROH compared to HOH, and the electron density of R is far greater than that of H; the dispersion interaction between the solvent electron density and the ring π-system becomes more significant in these instances. The ethanol clusters has many different calculated conformations due mostly to orientations of the ethyl group: basically the cluster geometry for 7AZI(CH₃OH)₁ and (C₂H₅OH)₁ clusters is similar.

G. 7-Azaindole/Ammonia Clusters. 7AZI clustered with ammonia has a spectrum different from both the bare molecule 7AZI and the other clusters, as presented in Figure 14. Note especially the low-lying vdW modes following within 50 cm⁻¹ of the 0^0_0 transition and the low-lying molecular vibronic features at ca. 200 and 400 cm⁻¹. The 7AZI(NH₃)₁ spectrum looks much
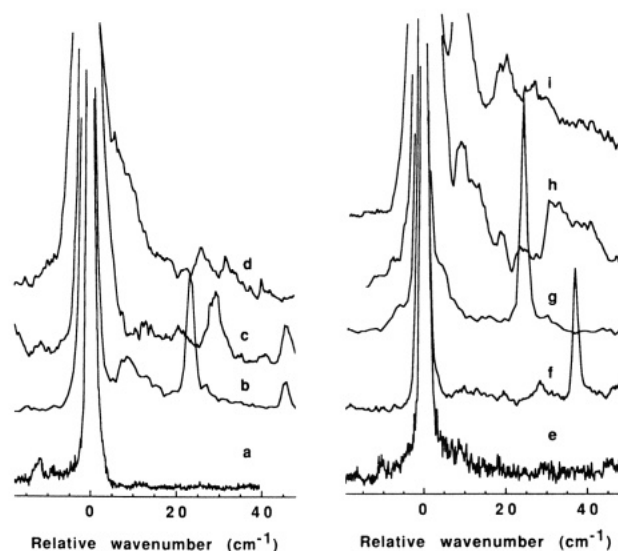

Figure 16. Comparison of the vdW modes built on the origins of various clusters: (a) 7AZI, (b) 7AZI(CH₃OH)₁, (c) 7AZI(Ar)₁, (d) 7AZI-(CH₄),1, (e) 7AZI(H₂O)₁, (f) 7AZI(H₂O)₂, (g) 7AZI(H₂O)₃, (h) 7AZI(NH₃)₁, (i) 7AZI(NH₃)₂.

TABLE V: Solvent Shifts for 0^0_0 Electronic Transition Energy of 7AZI

system	cluster shift/cm⁻¹	cluster binding energy[a]/cm⁻¹
7AZI	0	
7AZI(Ar)₁	−18	−345
7AZI(CH₄)₁	−46	−645
7AZI(H₂O)₁	−1288	−819
7AZI(H₂O)₂	−1997	−1630, −2760, −2900
7AZI(H₂O)₃	−2075	−3500 to ~−4500
7AZI(CH₃OH)₁	−1425	−1000, −1100
7AZI(CH₃OH)₂	−2376[b]	
7AZI(C₂H₅OH)₁	−1454, −1420, −1430	−1000 to ~−1200
7AZI(NH₃)₁	−1217	−930
7AZI(NH₃)₂	−1694	−1850, −1950
(7AZI)₂[c]	−2342	−2310

[a] Based on PM3 Hamiltonian to optimize 7AZI charges and geometry. [b] Reference 16. [c] Not shown in this paper.

simpler (i.e., has fewer transitions) than the 7AZI(H₂O)₁ spectrum.

According to the potential energy calculation, the NH₃ molecule coordinates to the aromatic π-system for the minimum energy configuration (see Figure 15). The 7AZI(NH₃)₂ cluster has the typical symmetric and asymmetric structures as depicted in Figure 15. The observed spectrum for 7AZI(NH₃)₂ is thought to arise from the symmetric structure because of the cluster shift, the large number (five) of different asymmetric structures generated in the calculation, and the fact that 80% of the calculated minimum energy structures are of the form displayed in Figure 15b.

H. van der Waals Modes for the *7AZI Clusters*. Figure 16 summarizes the vdW mode spectra for the various clusters. Note that in general the intensity of these features is weak and the Franck–Condon envelope for the transition has its maximum at the $\Delta\nu = 0$ position. Similar results are obtained for most vdW clusters.[31] None of the features above $0^0_0 + 100$ cm⁻¹ in the various clusters can be attributed to vdW modes.

I. Cluster Shifts. Cluster red shifts are large and probably more indicative of the $n\pi^*-\pi\pi^*$ residual mixing in the cluster than they are of solute/solvent interaction energy. For example, the shifts presented in Table V do not reflect hydrogen-bonding strengths. Moreover, the addition of a second solvent molecule also generates a large red shift in the disolvate cluster. Both observations seem to suggest that a planar double-hydrogen-bonded structure is not the lowest energy structure for these solute/solvent systems in the gas phase.

V. Summary and Conclusions

Results of these studies for 7AZI and its clusters with argon, methane, water, alcohols, and ammonia can be summarized as follows: (1) the spectrum of the bare molecule is quite congested with many low-energy vibronic features and apparent doublets appearing in the mass-resolved excitation spectrum; (2) the cluster spectra are also of the same nature but the vibronic structure is quite different for each particular cluster; (3) the vibronic doublets disappear upon deuteration of 7AZI at H_{10}; (4) calculations suggest that 7AZI may be nonplanar in S_1; (5) potential energy calculations suggest that cyclic hydrogen bonding between water, alcohols, and ammonia and 7AZI is not a stable low-energy structure for the first two solvent molecules in the cluster; and (6) all cluster spectra are red-shifted from the bare molecule origin, especially for polar solvents as indicated in Table V.

The conclusions we draw from these results are as follows: (1) strong $n\pi^*-\pi\pi^*$ vibronic mixing occurs between the ^1L_b $\pi\pi^*$ excited state and a lower lying $n\pi^*$ state; (2) this vibronic mixing is only partially removed by clustering; (3) a cyclic hydrogen-bonded structure is not achieved for the $7AZI(H_2O)_{1,2}$, $7AZI(ROH)_{1,2}$, or $7AZI(NH_3)_{1,2}$ clusters; and (4) the 7AZI molecule is nonplanar (at $H_{10}-N_1$ on the pyrrole ring) in the first excited singlet state.

The large spectral $S_1 \leftarrow S_0$ red shifts for water, alcohol, and ammonia 7AZI clusters do not necessarily imply a cyclic hydrogen-bonded cluster structure because the (supposed) stability of these structures would not correlate with the size of the red shift.

Finally, these results suggest that the double-hydrogen-bonding structures assumed to be intermediates in the 7AZI tautomerization process in condensed phases may only be present in rather high solvent density systems for which solvent molecules occupy the ring-centered solvation sites of 7AZI. Under such conditions, solvent molecules may occupy the lower binding energy hydrogen-bonded sites at the N_7 and N_1-H_{10} positions (see Figure 1a).

Au(0)–Ethylene and Au(0)–Dioxygen Complexes: Gold Nuclear Hyperfine and Quadrupole Coupling Tensors

Paul H. Kasai

IBM Almaden Research Center, San Jose, California 95120 (Received: September 22, 1989)

Powder pattern electron spin resonance spectra of the Au atom complexes of ethylene and oxygen molecules, $Au(C_2H_4)$ and $Au(O_2)$, show anomalies due to ^{197}Au nuclear quadrupole interactions. In the case of $Au(C_2H_4)$, owing to an extremely large nuclear hyperfine interaction, the quadrupole interaction is manifested as a subtle intensity variation in the powder pattern of the normal transitions. In the case of $Au(O_2)$, the hyperfine interaction is small, and the quadrupole term is manifested in the form of forbidden transitions. Both complexes have a side-on structure where the metal atom is situated equidistant from the ligand termini. The following quadrupole coupling tensors were determined through analyses of the powder patterns via simulation: for $Au(C_2H_4)$ $P_x = -2P_y = -2P_z = 100 \pm 15$ MHz, and for $Au(O_2)$ $P_z = -2P_x = -2P_y = 45 \pm 5$ MHz, where the z axis is parallel to the C–C or O–O bond of the ligand and the y axis is perpendicular to the plane of the complex. The electron distributions indicated by the quadrupole tensors are in accord with the structures and the bonding schemes envisaged for the respective complexes.
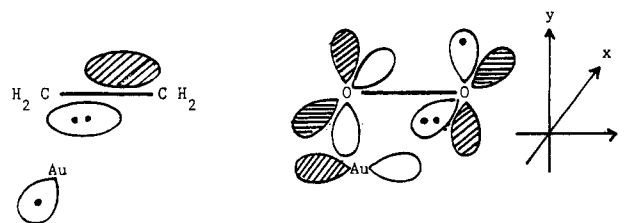
Introduction

Earlier we reported on ESR studies of mono- and bis(ethylene) complexes of Au atoms.[1] The complexes were generated by cocondensation of gold atoms and ethylene molecules in argon matrices at near liquid helium temperature. The ESR spectrum of Au(0)–monoethylene is characterized by an extremely large, essentially isotropic hf (hyperfine) coupling tensor of the ^{197}Au nucleus (natural abundance = 100%, $I = 3/2$, $\mu = 0.1439\beta_n$). The ESR spectrum of bis(ethylene)gold(0), on the other hand, is characterized by an orthorhombic g tensor of large anisotropy, and a relatively small but highly anisotropic ^{197}Au hyperfine (hf) coupling tensor. The ^{197}Au nucleus has an unusually large nuclear quadrupole moment ($Q = 0.594 \times 10^{-24}$ cm^2), and hence when its hyperfine interaction is small, conspicuous anomalies may be seen in the ESR powder pattern due to severe mixing of the nuclear spin states. Such anomalies are observed in the powder pattern of bis(ethylene)gold(0) and have been analyzed in detail.[2]

When the hyperfine interaction is extremely large compared to the nuclear quadrupole term, the effect of the latter upon the ESR powder pattern is almost negligible and difficult to discern. During our recent study of Au(0)–monocarbonyl, we noted and showed that, even in such a case, the quadrupole term causes a subtle but characteristic deviation in the powder pattern of the normal transitions, and it may be assessed with reasonable accuracy by spectrum simulation.[3]

Recently we also reported on the ESR spectrum of Au(0)–dioxygen complex.[4] Though ethylene and oxygen molecules are nominally "isoelectronic", and both $Au(C_2H_4)$ and $Au(O_2)$ complexes have similar symmetric side-on structures, the interactive schemes and dispositions of the unpaired electron in these complexes are totally different as depicted below.[1,4,5-7]

(1) Kasai, P. H. *J. Am. Chem. Soc.* **1983**, *105*, 6704.
(2) Kasai, P. H. *J. Phys. Chem.* **1988**, *92*, 2161.
(3) Kasai, P. H.; Jones, P. M. *J. Am. Chem. Soc.* **1985**, *107*, 6385.
(4) Kasai, P. H.; Jones, P. M. *J. Phys. Chem.* **1986**, *90*, 4239.
(5) McIntosh, D.; Ozin, G. A. *J. Organomet. Chem.* **1976**, *121*, 127.
(6) McIntosh, D.; Ozin, G. A. *Inorg. Chem.* **1976**, *15*, 2869.
(7) Howard, J. A.; Sutcliffe, R.; Mile, B. *J. Phys. Chem.* **1984**, *88*, 4351.